Elsevier Editorial System(tm) for Renewable Energy
Manuscript Draft

Manuscript Number: RENE-D-20-01002R2

Title: Experimental study of thermal fracturing of Hot Dry Rock irradiated by moving laser beam: temperature, efficiency and porosity

Article Type: Research Paper

Keywords: rock temperature; granite; thermal fracturing; laser irradiation; specific energy; open porosity

Corresponding Author: Dr. Yijiang Wang, Ph.D

Corresponding Author's Institution: China University of Ming and Technology

First Author: Yijiang Wang, Ph.D

Order of Authors: Yijiang Wang, Ph.D; Jinyi Jiang; Jo Darkwa, Ph.D; Zeyuan Xu, Ph.D; Xiaofeng Zheng, Ph.D; Guoqing Zhou, Ph.D

Abstract: A new laser irradiation fracturing method is employed to crack the Hot Dry Rock (HDR) and variations of rock temperature, specific energy (SE) and modified specific energy (MSE), thermal damages and open porosity of granite samples caused by moving laser beams with various irradiating conditions including laser power, diameter and moving speed of laser beam were investigated. Results indicate that rock temperature and the corresponding temperature gradients near the laser beam spots are strongly dependent on the laser power, beam diameter and irradiation time. The high temperature generated by the laser irradiation melts and cracks the HDR samples. The removed mass, cracked mass and size of grooving kerf induced by laser irradiation are also related to various irradiation conditions. SE and MSE are found nonlinearly reduced with the increased laser power density. Laser irradiation has a greater enhancement to thermal fracturing of granite than it does to thermal drilling. The open porosity (OP) of irradiated HDR samples increases with increasing laser power, decreasing diameter and moving speed of laser beam. The results can provide some guidance to those seeking a new economical and reasonable fracturing method for the HDR geothermal exploitation.

Highlights:

- A new graphite fracturing method by using laser irradiation is introduced.
- Effect of laser power, beam diameter and moving speed on cracking is studied.
- Graphite samples are melted and cracked by moving laser beam.
- Modified specific energy decreases with increased laser power density.
- Open porosity, removed and cracked mass depend on irradiation conditions.

Experimental study of thermal fracturing of Hot Dry Rock irradiated by moving laser beam: temperature, efficiency and porosity

Yijiang Wang [a,b]*, Jinyi Jiang [a], Jo Darkwa [b], Zeyuan Xu [b], Xiaofeng Zheng [b], Guoqing Zhou [a]*

[a] State key laboratory for Geomechanics and Deep Underground Engineering, School of Mechanics and Civil Engineering, China University of Mining and Technology, Xuzhou 221116, China

[b] Faculty of Engineering, University of Nottingham, University Park, Nottingham NG7 2RD, UK

Abstract: A new laser irradiation fracturing method is employed to crack the Hot Dry Rock (HDR) and variations of rock temperature, specific energy (SE) and modified specific energy (MSE), thermal damages and open porosity of granite samples caused by moving laser beams with various irradiating conditions including laser power, diameter and moving speed of laser beam were investigated. Results indicate that rock temperature and the corresponding temperature gradients near the laser beam spots are strongly dependent on the laser power, beam diameter and irradiation time. The high temperature generated by the laser irradiation melts and cracks the HDR samples. The removed mass, cracked mass and size of grooving kerf induced by laser irradiation are also related to various irradiation conditions. SE and MSE are found nonlinearly reduced with the increased laser power density. Laser irradiation has a greater enhancement to thermal fracturing of granite than it does to thermal drilling. The open porosity (OP) of irradiated HDR samples increases with increasing laser power, decreasing diameter and moving speed of laser beam. The results can provide some guidance to those seeking a new economical and reasonable fracturing method for the HDR geothermal exploitation.

Keywords: rock temperature; granite; thermal fracturing; laser irradiation; specific energy; open porosity

Nomenclature

L	length of the sample (m)
m	mass of rock sample (kg)
m_s	mass of saturated rock sample irradiated by laser (kg)
m_d	mass of dry rock sample (kg)
N	number of testing samples
P_{out}	laser power (W)
r	radius of the rock sample (m)
SE	specific energy (kJ/cm^3)
MSE	modified specific energy for laser fracturing (kJ/cm^3)
t	irradiation time (s)
u_v	uncertainty of directed variables
$\triangle_v$	test accuracy of the variables
V_c	volume of cracked rock (cm^3)
V_r	volume of removed rock (cm^3)
$\bar{x}$	mean value of individual testing values
x_i	individual testing values

Greek symbols

η	water saturation (%)
ρ	density of rock sample (kg/m^3)
ρ_d	density of dry rock sample (kg/m^3)
ρ_w	density of water (kg/m^3)
σ_v	Bessel equation of standard deviation
φ	saturated water content of original rock sample
φ_o	open porosity of irradiated rock sample

1. Introduction

"Hot Dry Rock (HDR) geothermal energy is a type of green and renewable resource" stored in deep granite strata [1, 2]. The "exploitation and utilization of HDR geothermal energy" have attracted wide interest due to being non-polluting and environmentally friendly. For instance, the total installed capacity of geothermal energy plants around the world achieved 14.3 GWe in 2017 [3], and the total amount of directly utilized geothermal energy in China also reached 17870 MWt in 2014. In addition, more potential has also been observed in hybrid power system based on other renewable energy sources in the future [4]. Technology improvements of geothermal reservoirs should be given more attention to achieve sustainable development of geothermal energy [5, 6].

One of the key parameters in exploitation of geothermal energy is the rock permeability. Thermal cracking and hydraulic fracturing are usually used by researchers and engineers to significantly change physical properties which can improve the permeability and accelerate the fracture propagation. A series of lab-based block tests have been performed by Hu et al [7] to examine the effect of reservoir stimulation on enhanced geothermal system by characterizing the fracture and assessing the system enhancement through hydraulic fracturing. Results indicated that hydraulic fracturing resulted in the fracture aperture with a rough surface. Ma et al [8] studied the factors that had impact on crack extension using a 3D hydraulic fracturing model. It was found that the impact of the fluid displacement was greater on the fracture morphology than on viscosity and "main crack of HDR was more sensitive to rock elastic modulus than horizontal in-situ stress difference". How cracks are developed in the granite in an environment with high temperature and pressure was investigated by Zhao et al [9-12] who discovered that the failure mode was either "shear failure or a combination of shear and tension failure". In addition, heating from the critical temperature resulted in the considerably increased permeability of granite. And inter-granular micro-cracks were observed at grain boundaries owing to the effect of thermal cracking, and develops a long apparent weakness with increasing temperature. Thermal cracks are the leading cause for the change of permeability paralleled to bedding, and the increase in permeability perpendicular to bedding was caused by the connection of macropores [13]. Huang et al [14, 15] concluded that rock temperature was one of the key factors that affect hydraulic breakdown pressure. Additionally, the seepage capacity could be affected by confining pressure and rock roughness.

As a matured technology, laser beams have been widely applied to metal and non-metal processing due to their high energy density within a small area where the beam is focused. A large number of experimental and numerical investigations have been carried out in the metal or non-metal manufacturing industry based on laser cutting or welding, which show that the overall processing performance mainly depends on the laser power, irradiation time or pulse duration [16-21].

Potentially, high power laser beams could also be applied to the rock stimulating to improve the permeability and drilling speed especially in gas and oil engineering. One of the earliest researches on the laser excavation was conducted by Jurewicz [22] who used high power laser machine to excavate hard rock and this method showed some advantages such as increased excavation speed and good cracking efficiency. The variation of specific energy was investigated by Ahmadi et al [23] who employed a Nd:YAG laser to perforate rock samples saturated with water and heavy oil. Results showed that the penetrated depth of rock hole was increased by irradiation time, and the required amount of specific energy for water saturated rock sample was more than that for both heavy oil saturated and dry samples. Erfan et al [24] investigated the moving laser perforation of rocks by using long pulse Nd:YAG laser with a vertical speed that was equal to the perforation rate. It was found that the efficiency was optimal for moving laser perforation. Hu et al [25] reported laser perforation in oil and gas wells and investigated the temperature distributions on the rock surfaces after laser irradiation both experimentally and numerically. They found that the size and deposition orientation of the rock had no impact on perforation efficiency when the boundary effects were eliminated. The impact of water on perforation rate, specific energy has been investigated by Kariminezhad et al [26] through experimental study, which assessed the concrete perforation with the assistance of a continuous CO_2 laser. Results showed that the presence of moisture had a significant incremental and detrimental impact on the perforation rate and specific energy, respectively. Keshavaizi [27] employed high-power laser to perforate and fracture rock of oil and gas well to increase the permeability to take the place of the costly post-perforation operations. High power laser was used to experimentally analyze a number of key indicators such as the sandstone fracture morphologies, quantitative characterization, specific energy and perforation rate [28]. When the laser power increased, cracks were formed and developed along the inner wall. Further analysis revealed the specific energy decreased gradually but the perforation rate increased instead. Lyu et al [29] developed a specific energy model for thermal spallation drilling on six types of rocks and identified the importance of controlling the velocity of the coiled tubing to delivering the optimum penetrating rate during spallation drilling. Results also demonstrated that the thermal spallation drilling is a suitable alternative for the exploitation of oil and gas in hard rocks. Miranda [30] suggested that CO_2 laser can be used to cut marble and limestone and the quality of the cut surface largely depended on the stone’s chemical and mineralogical compositions. Ng et al [31] built an analytical model to understand the impact of various factors such as "the velocity of melt ejection, the drilling rate, the contributions of melt ejection and vaporization to the overall drilling rate". The impact of the pulse format on the drilling performance was investigated through numerical and experimental studies by Shin et al [32] where the key interaction physics between laser and material were emulated, such as heat transfer, vaporization, fluid flow, and multiple reflections. In a study by Yan et al [33], the interaction mechanism of rock perforation by laser irradiation was introduced to study the laser penetration at different depths and it was found that laser power and irradiation time affected the perforation the most. The thermal and mechanical characteristics of limestone rock, which was irradiated by continuous wave fiber laser with different laser power, were experimentally investigated by Wang et al [34]. Based on aforementioned literatures, the technical comparison between hydraulic and laser irradiation fracturing is summarized in Table 1, which indicates that laser irradiation is a suitable measure with higher performance for rock fracturing.

Table 1. Comparison between hydraulic and laser irradiation fracturing.

Parameters	Hydraulic	Laser irradiation
Fundamental	High-pressure water	High-power laser
Efficiency	High [15]	Superhigh [28]
Specific energy	Low [7]	Extremely low [34]
Directional	Poor [1]	Excellent [27]
Environmental	Risk of pollution [8]	Friendly [28]

A large number of investigations have been carried out on the high-efficient exploitation of HDR geothermal energy based on hydraulic fracturing and exploitation of gas or oil based on hybrid technology combining hydraulic fracturing and laser drilling and cracking. And it can be observed that the previous studies were focused mainly on laser drilling efficiencies and rates of perforation. The investigation on the mechanism and efficiency of HDR fracturing by laser irradiation, especially with the assistance of moving laser beam, has been less reported so far. Therefore, this paper presents experimental investigations on how laser power, laser beam diameter and moving speed of laser beam affect the variations of rock temperature, thermal fracturing efficiency and open porosity. The experimental results can be used to evaluate the fracturing efficiency of granite rock with the assistance of moving laser beam and can also be used to validate a theoretical prediction of the temperature field created by laser irradiation.

2. Specimen and experimental system

2.1. Specimen

The standard granite samples, with diameter and length of Φ50mm×100mm, are used as the specimen in this investigation. The samples are prepared with ground flat ends to reduce the test error of thermal conductivity and compressive strength. The overall structure of the granite samples is compact and uniformly granular. As shown in Table 2, the main minerals of the granite samples are quartz, albite, potassium feldspar, and iron dolomite. The average thermal conductivity and compressive strength of the granite samples are 3.401 W/mK and 134.95 MPa respectively, and other physical-mechanical properties such as density, moisture content are also illustrated in Table 3.

Table 2. The components of the granite sample.

Mineral	Na_2O	MgO	Al_2O_3	SiO_2	K_2O	CaO	Fe_2O_3	Others
Mass fraction/%	3.53	0.69	13.91	68.55	5.16	1.63	2.46	4.07

Table 3. The physical parameters of the granite sample.

Density (kg/m^3)	Heat capacity ($kJ/m^3\cdot K$)	Thermal conductivity (W/mK)	Compressive strength (MPa)	Tensile strength (MPa)	Moisture content (%)	Saturated moisture content (%)
2580	997.1	3.401	134.95	12.36	0.054	0.142

2.2. Experimental setup

A continuous fiber laser (nLight, USA) with maximum output power of 1 kW is applied to irradiate the granite samples. The laser is conducted to a laser cutting head (Lasermech, USA) through glass fiber cable and the cutting head is mounted on an industrial six axles robot (ABB, Switzerland), as shown in Fig. 1. The movement of the laser cutting heads is automatically controlled by the robot during experiments for safety. The technical specifications of the fiber laser system are presented in Table 4. An infrared camera (Flir, USA) with a temperature measurement up to 2000 ^{o}C is applied to measure the granite sample surface temperature directly during laser beam irradiation experiment and the images are recorded and presented in this paper in the following sections. The accuracy of temperature measurement is less than ±2 ^{o}C or within ±2% of the measured value.

Fig. 1. The fiber laser system.

Table 4. The technical specifications of laser system.

Parameters	Values
Mode of operation	CW/modulated
Polarization	random
Maximum average power	1 kW

Power variation (8-hour)	≤1%
Rise and fall times	≤ 5 μm
Beam quality	≤ 2 mm-mrad (50 μm fiber) ≤ 4 mm-mrad (100 μm fiber) ≤ 11 mm-mrad (200 μm fiber)
Wavelength	1080 ± 10 nm
Spatial freedom of ABB industrial robot	6 axles
Positioning accuracy of ABB industrial robot	±0.01 mm

Thermal conductivity of the specimen is measured by a thermal constant analyser (Hot Disk, Sweden). Both X-Ray Fluorescence (XRF, Bruker, Germany) and X-Ray Diffraction (XRD, Bruker, Germany) are employed to analyze the components of the granite specimen. The compressive strength of granite specimen is tested by using an YNS2000 electro-hydraulic servo universal testing machine (Sino-test, China) with the maximum load of 2000 kN and the testing accuracy of ±1% full scale. The mass and size of granite specimen are measured by an electronic balance (Yingheng, China) with accuracy of 0.01g and a digital caliper (Deli, China) with accuracy of 0.01 mm respectively. The width and depth of the grooving kerf are also measured by the same digital caliper.

2.3. Experimental program

A granite specimen is fixed on a test bench horizontally and the laser cutting head is mounted on an arm of the robot vertically over the specimen, as shown in Fig. 2. It is moved from left to right parallel to the specimen under controlled speed. High power laser beam from the cutting head irradiates on the top surface of specimen directly. The heat generated by the laser beam can melt the specimen and result in a deep grooving kerf on the top of the rock sample. Liquidation and gasification can be observed during the laser beam irradiation experiment from Fig. 1, and cracks can also be observed after the irradiation due to high temperature gradient within the specimen. The most important parameters of laser irradiation are laser power and irradiation time [33]. A series of experiments are conducted with varied laser power, laser beam diameter and moving speed of laser beam as shown in Table 5. The effects of laser power, laser beam diameter and translational speed of laser beam on rock temperature, thermal drilling and fracturing efficiencies, grooving kerf size are therefore studied and presented in this paper.

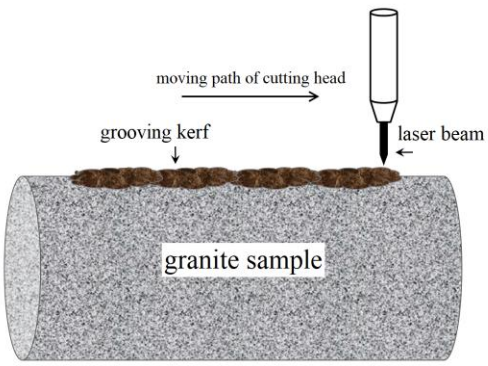

Fig. 2. Sketch of moving laser irradiation.

Table 5. The experimental program.

Parameters	I	II	III	IV
Laser output power (W)	400	600	800	1000
Laser beam diameter (mm)	6	8	10	12
Translational speed of laser beam (mm/s)	0.5	1.0	2.0	4.0

2.4. Experimental data processing and uncertainty analysis

The granite sample density is described by Eq. (1):

$$\rho = \frac{m}{\pi r^2 L} \tag{1}$$

where ρ is the density of sample (kg/m^3), m is the mass of sample (kg), r and L are the radius and length of the sample respectively (m).

Several parameters are employed in order to compare the effects of laser irradiation on thermal drilling and fracturing of granite rock. For example, the specific energy (SE) is defined as the total laser energy divided by the volume of removed rock by laser irradiation directly [23]:

$$SE = \frac{P_{\mathrm{out}} \cdot t}{V_{\mathrm{r}}} \tag{2}$$

where SE is the specific energy for thermal drilling (kJ/cm^3), P_{out} is the power of laser beam (W), t is the irradiation time (s), V_{r} is the volume of the rock removed by the laser irradiation directly (cm^3).

The modified specific energy is defined as the total laser energy divided by the total volume of cracked rock from the specimen by laser irradiation, which can be expressed by [34]:

$$MSE = \frac{P_{\mathrm{out}} \cdot t}{V_{\mathrm{c}}} \tag{3}$$

where MSE is the modified specific energy for thermal fracturing (kJ/cm^3), V_{c} is the volume of cracked rock from specimen by laser irradiation (cm^3).

The open porosity of the irradiated rock sample is defined as:

$$\varphi_{\mathrm{o}} = \frac{m_{\mathrm{s}} - (1+\eta) m_{\mathrm{d}}}{\rho_{\mathrm{w}}} \Big/ \frac{m_{\mathrm{d}}}{\rho_{\mathrm{d}}} \tag{4}$$

where φ_{o} is the open porosity of irradiated rock sample (%) , m_{s} and m_{d} are respectively the mass of saturated and dry rock sample that is subject to irradiation (kg), ρ_{w} is the density of water (kg/m^3), ρ_{d} is the density of dry rock sample (kg/m^3), η is the saturated water content of rock sample (%).

In order to ensure the accuracy of the experimental results, the testing accuracy and uncertainty of the experimental setup are analyzed. The equations of uncertainties for directed variables including mass, length are present by [35]:

$$u_{\mathrm{v}} = \sqrt{\Delta_{\mathrm{v}}^2 + \sigma_{\mathrm{v}}^2} \tag{5}$$

where u_{v} is uncertainty of directed variables, $\triangle_{\mathrm{v}}$ is the test accuracy of the variables, σ_{v} is the Bessel equation of standard deviation and the equation is described by Eq.(6):

$$\sigma_{\mathrm{v}} = \sqrt{\frac{\sum_{i}^{N}\left(x_i - \bar{x}\right)^2}{N-1}} \tag{6}$$

where x_i and $\bar{x}$ are individual testing values and the mean value of individual testing values, N is the number of testing items.

The equations of uncertainties for undirected variables, such as density, SE/MSE and open porosity are described by Eq.(7) and Eq.(8) [35]:

$$u_{\mathrm{v}}^{'} = \sqrt{\sum_{i}^{n}\left(\frac{\partial F}{\partial x_i} \cdot \Delta_{x_i}\right)^2} \tag{7}$$

$$u_{\mathrm{v}}^{'} = \sqrt{\sum_{i}^{n}\left(\frac{\partial \ln(F)}{\partial x_i} \cdot \Delta_{x_i}\right)^2} \tag{8}$$

where $u_{\mathrm{v}}' = F(x_i)$ is undirected variable calculated from x_i. The equation (7) should be used to calculate the uncertainties if the $F(x_i)$ just includes operators of add and subtract, and equation (8) is used if the $F(x_i)$ just includes operators of multiplication and division.

According to Equations (5)-(8), the testing accuracy and uncertainty of variables are listed in Table 6. The uncertainties of temperature, SE/MSE and open porosity are about ±2%, 2%~5% and 2%~5% respectively, which verifies that the testing accuracy of the experimental results can be ensured.

Table 6. Testing accuracy and uncertainties.

Variables	Temperature	Mass	Length	Volume	SE/MSE	Open porosity
Testing accuracy	±2%	±0.01 g	±0.02 mm	-	-	-
Uncertainty	±2%	2%~5%	0.11%	0.08%	2%~5%	2%~5%

In addition, the standard deviation is also calculated to quantify the divergence of testing values. The equation of standard deviation S_N is shown as follows:

$$S_N = \sqrt{\frac{1}{N}\sum_{i=1}^{N}(x_i - \overline{x})^2} \tag{9}$$

3. Results and discussions

A series of experiments are conducted to the same granite samples under various laser power, laser beam diameters and moving speed of laser beam. The effects of various irradiation conditions on rock temperature distributions are presented firstly, followed by the effects on the laser drilling and thermal fracturing efficiencies, and finally different grooving kerf sizes and open porosities of irradiated rock samples are compared. The granite samples used in the experiments are made from the same rock and the difference of the minerals inside the samples were negligible. Therefore, the influences of sample minerals on experiments are not appraised in this investigation. In addition, the variations of compressive strength, cracks distribution, permeability and acoustic emission results are also not analyzed in this manuscript and will be assessed and reported in another study.

3.1. Temperature distributions under various irradiation conditions

3.1.1. Laser power

Fig. 3 shows the changes of rock temperature at different irradiation times with laser power of 400 W, laser beam diameter of 6 mm and the laser beam moving speed of 0.5 m/s. These are the raw images obtained by infrared camera over the laser irradiation period of experiment. It can be seen from Fig. 3 (a) that rock temperature at the area where laser beam irradiated rapidly rises above 2000 ^{o}C almost immediately after laser beam irradiated. According to our previous experimental results, the surface temperature of rock near the laser beam reaches 2000 ^{o}C when the irradiation time approaches about 140 ms with the irradiation power of 800 W [34]. The hot spot with highest temperature moves along the specimen when laser beam moves at the speed of 0.5 m/s, which can be seen from images selected at the irradiation times of 40, 80, 120 and 160 s as shown in Fig. 3 (b)-(e). The maximum spot temperature is observed to be slowly decreased when laser beams is switched off and Fig. 3 (f) shows the maximum temperature drops to about 905 ^{o}C at 200 s (40 s after the irradiation is stopped). Also from Fig. 3 (b)-(e), one can see a clear low temperature tail is generated following the line of the hottest spot movement while the laser beam is constantly travelling along the sample. This indicates that the temperature created by the laser irradiation is above the melting point of the granite rock sample and the granite is melted at the hottest irradiated area. After the laser beam is moved away, the heat is conducted internally and dissipated to environment. The temperature drops down and the molten rock then becomes solid again. In addition, the length of the tails is proportional to the irradiating time and the temperature along the tail is gradually reduced as the distance from the hot spot is increased. Although there is no thermal energy from laser beam to continually irradiate the rock sample, the maximum rock surface temperature is also more than 900 ^{o}C. The reason is that the heat capacity of granite sample is much larger, meantime the convection coefficient of natural cooling is very small.

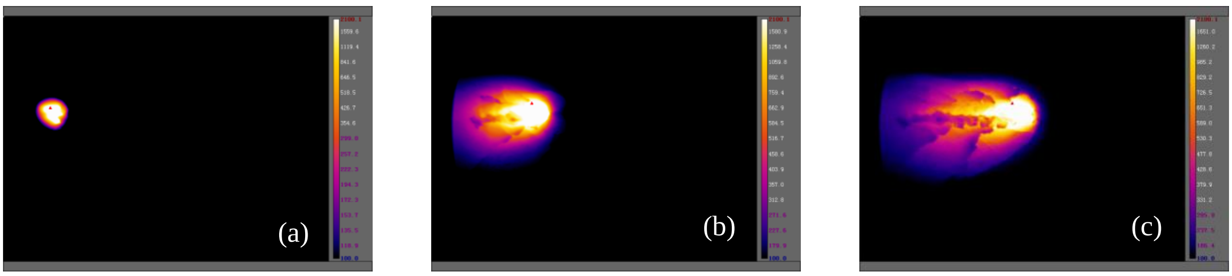

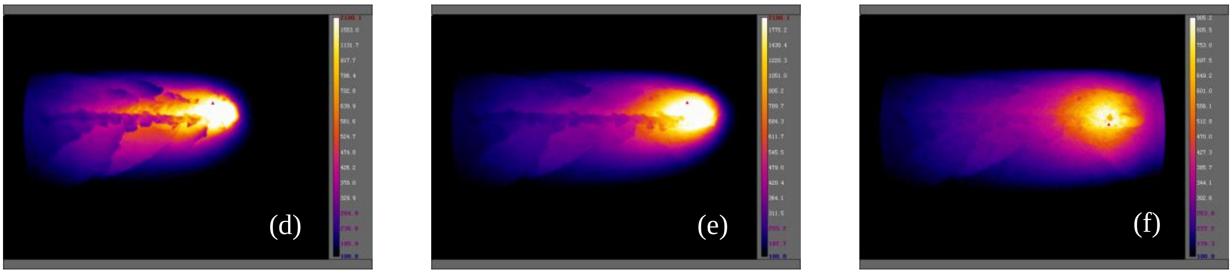

Fig. 3. Rock temperature at different time (a) 0s (b) 40s (c) 80s (d) 120s (e) 160s (f) 200s.

Fig. 4 shows temperature profiles at 160 s and 200 s obtained under different laser power, which ranges in 400 - 1000 W for the same laser beam diameter of 6 mm and laser beam moving speed of 0.5 mm/s. The temperature profiles are taken from the central line along the specimen axis in line with the laser beam center and moving direction. As can be seen from Fig. 4 (a), the length of high temperature region increases with laser power. For instance, the lengths of the hot spot with temperature higher than 2000 ^{o}C are 14.49 mm, 19.25 mm, 20.68 mm, 37.97 mm for the laser power of 400 W, 600 W, 800 W, and 1000 W respectively. Although the laser beam diameter is kept the same, as the laser power is increased, more thermal energy is generated in the irradiated area and heats a much larger area on the specimen surface. Temperature gradient at the frontier of laser spotted area is found proportional to the laser power from Fig. 4 (a). For instance, the temperature gradients are 2669 ^{o}C /mm, 2835 ^{o}C /mm, 3037 ^{o}C /mm, 3392 ^{o}C /mm for laser power of 400W, 600W, 800W and 1000W. Also we can see from Fig. 4 (a), in the region following the moving hot spot, a higher temperature can be found as the laser power is increased, and then a longer rock solidification time is expected for higher laser power irradiation case and a deeper or wider grooving kerf can be expected as well.

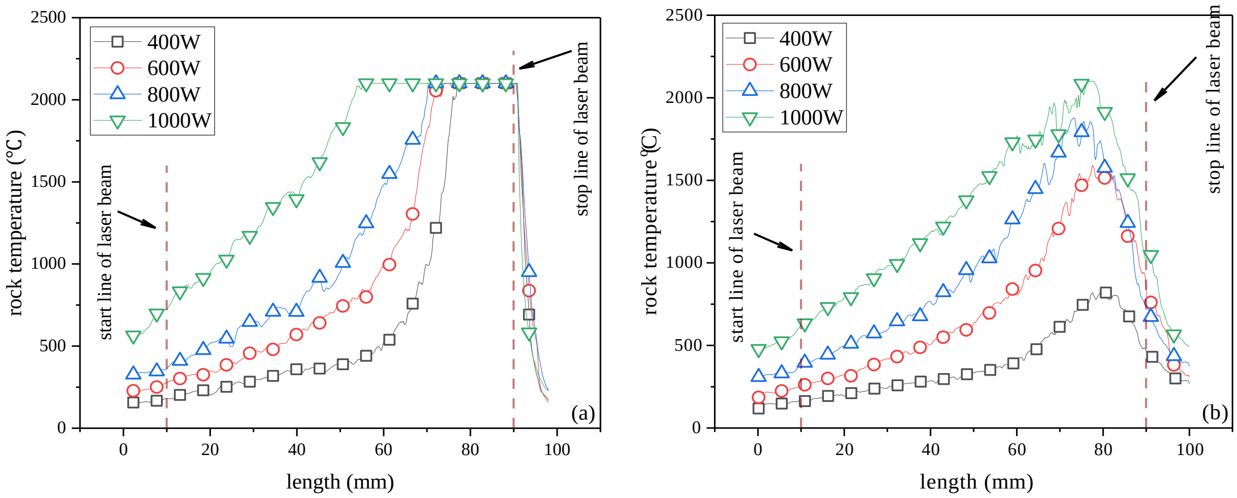

Fig. 4. Rock temperature distribution versus laser power (a) 160s (b) 200s.

The temperature profiles obtained at 40 s after switching off the laser beam for different laser power are shown in Fig. 4 (b). No forced cooling is applied to avoid any thermal crunching of specimen and the heat is dissipated to the environment naturally. The maximum rock temperature remains over 2000 ^{o}C for the 1000W case in the irradiated area, but the temperature decreases to about 750 ^{o}C for the case of 400 W. Comparing the length of region over 500 ^{o}C in the central line, it is increased from 23.26 mm, 57.04 mm, 74.33 mm to 96.26 mm for laser output power of 400 W, 600 W, 800 W and 1000 W respectively. With a higher-power laser beam, more heat is generated in the irradiated specimen and results in a larger high temperature area and higher temperature gradient around the hot spot which may cause more damages to the granite samples.

3.1.2. Laser beam diameter

As shown in the Table 2, experiments with different laser beam diameters at the same laser power and moving speed of laser beam are conducted in order to investigate the effect of laser beam diameter on the thermal damages of the same rock samples. Fig. 5 shows temperature contours of the experiments obtained at the laser power of 1000 W with a beam diameter of 6 mm and laser beam moving speed of 0.5 mm/s.

As shown in Fig. 5, the comparisons are made between the temperature contours obtained with different beam diameters at 160 s, which is the last second of the laser irradiation experiment. It is chosen to provide the longest irradiation time to make the effects more obvious. It’s interesting to see that as the laser beam diameter is increased, the hot spot area on the specimen is reduced for the same laser power. This is because for the same power of laser beam, when the beam diameter is doubled, the surface power density irradiated on the rock sample surface is reduced down to one quarter and the thermal energy at the surface is less concentrated. Also, one can see that for a small diameter beam, a large area of high temperature tail region is remained following the movement of hot spot. However, for a large beam diameter, the rock temperature at the tail regions is much lower and uniform. This may affect the performances of thermal fracturing on the granite rock. In addition, the regular variation of temperature gradient near the laser spot ranges between 3392-5064 ^{o}C/mm for different laser beam diameters.

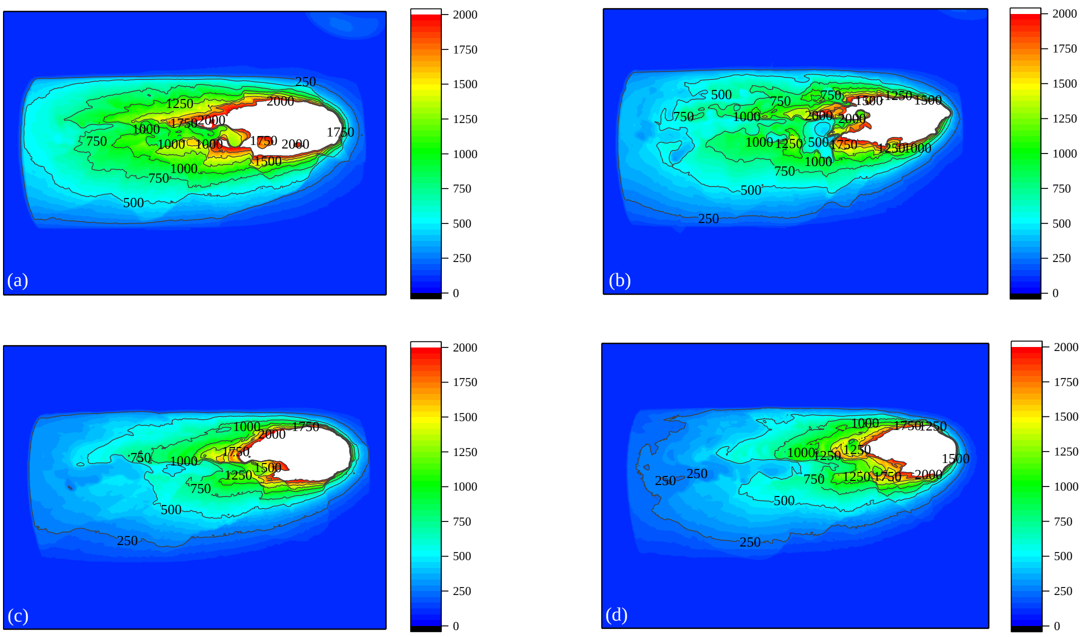

Fig. 5. Rock temperature versus beam diameter (a) 6mm (b) 8mm (c) 10mm (d) 12mm.

Fig. 6 shows a quantified comparison of laser beam diameter on the hot spot area of specimen in details obtained at irradiation time of 160 s and 200 s (40 seconds after laser is switched off). At the irradiation time of 160 s, the lengths of region with rock temperature higher than 2000 ^{o}C are decreased from 42.66 mm, 34.64 mm to 32.52 mm and 29.97 mm when laser beam diameter is increased from 6 mm, 8 mm to 10 mm, 12 mm, and the lengths of region with temperature higher than 1000 ^{o}C are also decreased from 59.88 mm, 48.64 mm to 34.49 m and 8.87 mm respectively after 40 seconds of natural cooling. This indicates that the length of region with higher temperature is increased as the laser beam diameter is decreased which results in larger thermal energy density on the irradiated area.

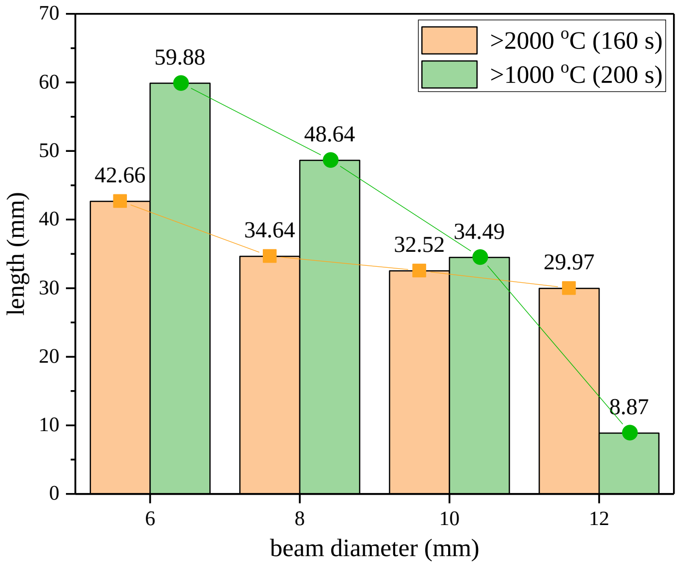

Fig. 6. Length of the high temperature region.

3.1.3. Translational speed of laser beam

With the same laser beam diameter of 6 mm and irradiation power of 1000 W, several experiments are conducted at varied laser beam moving speeds including 0.5 mm/s, 1.0 mm/s, 2.0 mm/s and 4.0 mm/s. Temperature contours obtained from the infrared thermal images at the end of the laser irradiation are shown in Fig. 7. When the moving speed of laser beam is doubled, the total thermal energy injected from laser beam onto the granite rock sample is reduced by 50% as the total energy is proportional to total irradiation time given the same laser power. One can expect a less thermal fracturing damage on the rock sample when the moving speed of laser beam is increased. As can be seen from Fig. 7 (a)-(d), the irradiation time of 160 s and 20 s is required to cover the same length on rock sample when the moving speed is 0.5 mm/s and 4mm/s respectively. The total thermal energy injected on the sample with the moving speed of 0.5 mm/s is eight times higher than that with the speed of 4 mm/s. The hot spot area over 2000 ^{o}C in the temperature contour of Fig. 7 (a) with moving speed of 0.5 mm/s is observed to be much larger than that with other three moving speeds shown in Fig. 7 (b)-(c). In addition, the shape of high temperature area is narrower and heating area is much smaller when the moving speed is increased. The thermal damages are expected to be increased with decreased moving speed of laser beam because of larger variation of total thermal energy injected on the sample surface.

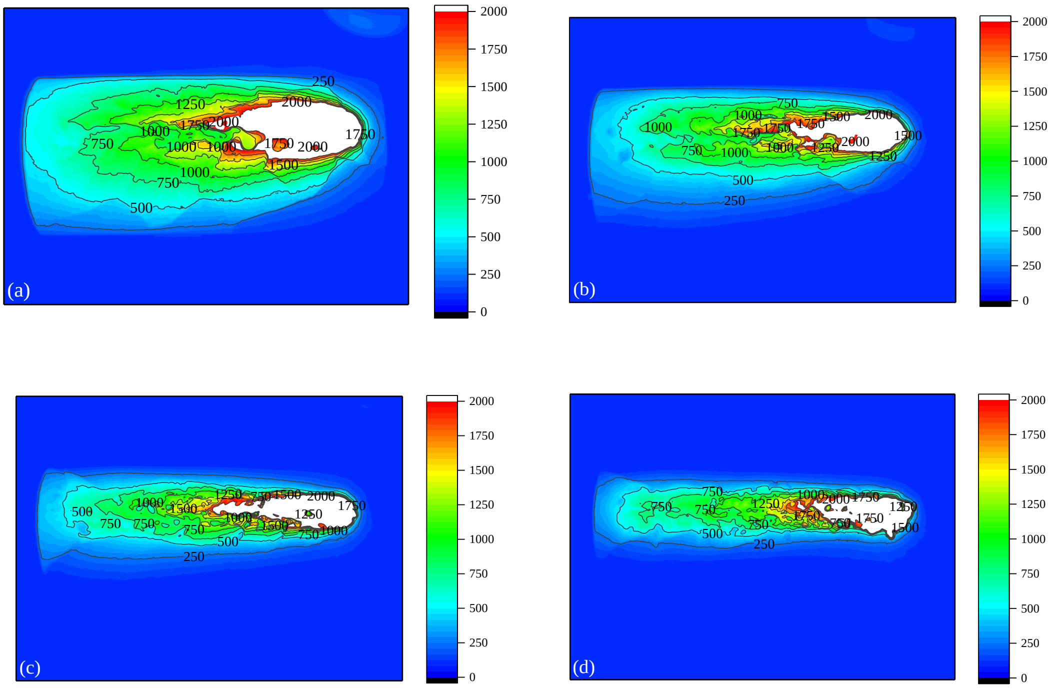

Fig. 7. Rock temperature versus moving speed (a) 0.5mm/s (b) 1mm/s (c) 2mm/s (d) 4mm/s

Fig. 8 shows the temperature profiles at the center of the rock samples with the four different moving speeds, which are obtained at 20 s after the laser beam is switched off. The specimen is cooled naturally. It can be seen that for the case of 0.5 mm/s, the rock temperature remains over 2000 ^{o}C in a large area after 20 seconds natural cooling time. The length of profile at temperature over 2000 ^{o}C is much longer than that of 1 mm/s. When the moving speed is increased to 2 mm/s, the maximum temperature of the sample surface is limited to 1850 ^{o}C after 20 s natural cooling and the maximum temperature is dropped down to 1200 ^{o}C when the moving speed is set up to 4 mm/s. It's also interesting to observe that the maximum temperature gradient at the leading edge of hot spot remains high after 20 seconds natural cooling, and the temperature gradient is reduced from 5700 °C/mm to 4800 ^{o}C/mm when the moving speed is increased from 0.5 mm/s to 4 mm/s.

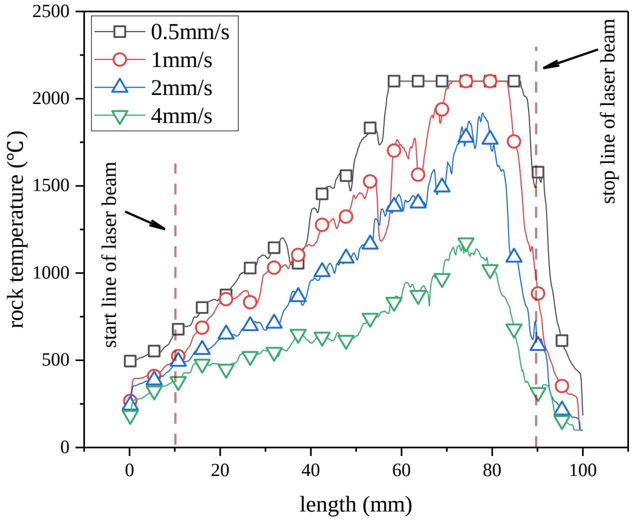

Fig. 8. Rock temperature distribution after natural cooling for 20s.

Due to the fact that rock temperature induced by laser irradiation is higher than the melting points of SiO_2 (1713 ^{o}C), $K[AlSi_3O_3]$ (1290 ^{o}C), $Na[AlSi_3O_3]$ (1215 ^{o}C) and biotite (1800 ^{o}C) which are the main components of granite sample, a clear grooving kerf matching with laser beam movement is observed after each experiment and the effects of laser power, laser beam diameter and moving speed of laser beam on the kerf are introduced in the following sections.

3.2. Efficiencies of laser drilling and thermal fracturing

3.2.1. Mass of removed and cracked rock

Owing to the high-power laser irradiation on the granite rock sample surface, local temperature at the irradiated surface is well above 2000 ^{o}C that is higher than the melting points and gasification temperature of some components in the granite rock. Heavy smoking is observed during the laser irradiation for almost all experiments and an example is shown in the Fig. 1. Glassification scars on the specimen remained at the bottom of grooving kerf provide evidence of rock melting during the laser irradiation. By comparing the mass of specimen before and after laser irradiation, one can find the mass of removed rock through gasification, where some liquid mass blown away by assistant gas is also included due to being unable to be separated. Fig. 9 shows the mass of removed rock by the laser irradiation under various conditions and the relation of mass reduction of irradiated samples with laser power, laser beam diameter and laser beam moving speed. Another investigation of laser irradiation on granite sample is to analyze the mass of cracked rock under different irradiation conditions. The cracked mass is defined as the total mass of all broken parts dropped off from the specimen after laser irradiation without any extra force as included in Fig. 9. The rock is broken because of high thermal stress within specimen induced by local high temperature gradient around the laser beam where a great amount of heat is generated [34].

As we can see from Fig. 9 (a), both removed mass and cracked mass of the granite specimen are significantly increased by higher laser power with the same laser beam diameter (6mm) and moving speed (0.5 mm/s). This is because with high power laser beam, more heat is generated on the same size of laser beam and causes more damages to the rock sample. However, when the laser beam diameter is increased, both gasification and damages on rock sample are reduced, as shown in Fig. 9 (b). This is because when the laser beam diameter with the same power is increased, the power density at the beam spot is significantly reduced and temperature gradient inside the specimen is reduced as well. The moving speed of laser beam also has a negative effect on the thermal damages as shown in Fig. 9 (c) when the laser speed is increased from 0.5 mm/s to 4 mm/s. As we can see from the profiles shown in Fig. 9, all these effects of laser power, laser beam diameter, and moving speed are non-linear.

Comparing the total removed mass with the cracked mass shown in Fig. 9 under all conditions, the cracked rock mass is about one or two orders higher than the mass of removed rock. And the gap between cracked and removed mass increases with the increase of laser power, decreases of laser beam diameter and moving speed. It suggests that using laser beam to crack rock is much more efficient than using laser beam to drill holes. If a laser beam is applied to rock fracturing or well drilling in oil and gas industry, a high-power laser with small diameter and lower moving speed is good choice.

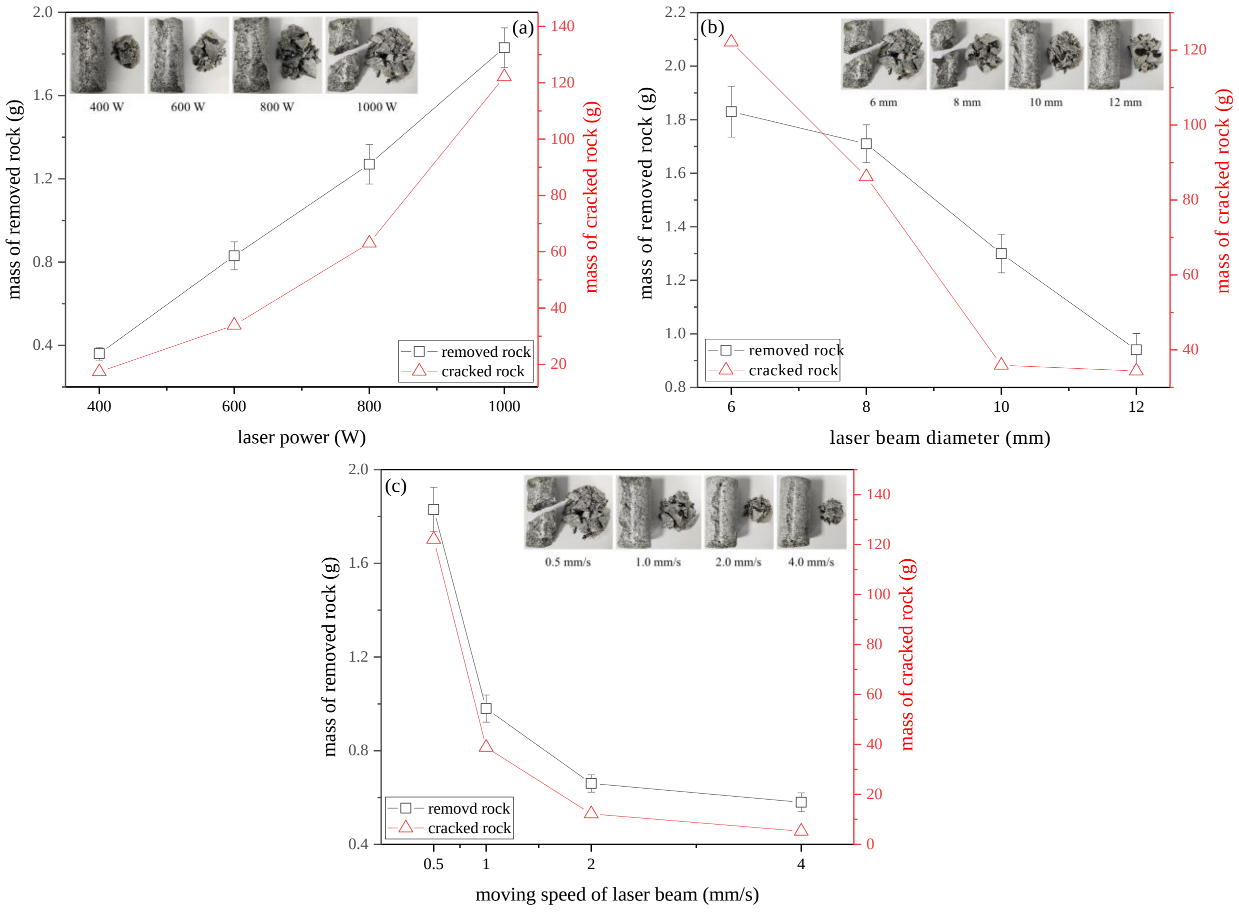

Fig. 9. Mass of removed and cracked rock versus (a) laser power (b) beam diameter (c) moving speed.

3.2.2. Specific energy and modified specific energy

Defined by Equations (2) and (3), the SE and MSE for each laser irradiation experiment are calculated and the detailed results are illustrated in Fig. 10. Fig. 10 (a) shows that the SE nonlinearly decreases with an increasing laser power. For instance, the SE decreases from 460 kJ/cm^3 to about 230 kJ/cm^3 when laser power is increased from 400 W to 1000 W, which indicates that less thermal energy is needed to remove the same quantity of rock or to drill the same depth of hole when laser is used in oil or gas well drilling. Therefore, using a high-power laser is much better than using a low-power laser for oil well drilling application. The SE can be seen nonlinearly increasing against laser beam diameter from Fig. 10 (b). The SE increases from 225 kJ/cm^3 with a laser beam diameter of 6 mm to about 440 kJ/cm^3 with a laser beam diameter of 12 mm. To improve the efficiency of thermal drilling, a smaller beam diameter should be used. That also means the distance between the cutting head and rock sample should be equal or close to the laser focal length which gives smaller diameter spot at the irradiation surface. Fig. 10 (c) shows that the SE also nonlinearly decreases with the increasing moving speed of laser beam. For instance, the SE is 227 kJ/cm^3 with a moving speed of 0.5 mm/s compared with 90 kJ/cm^3 with a moving speed of 4.0 mm/s. A slower moving speed of laser beam should be selected if removing more rock takes the priority. However, a quicker moving speed could be considered if the higher efficient of laser drilling is the priority.

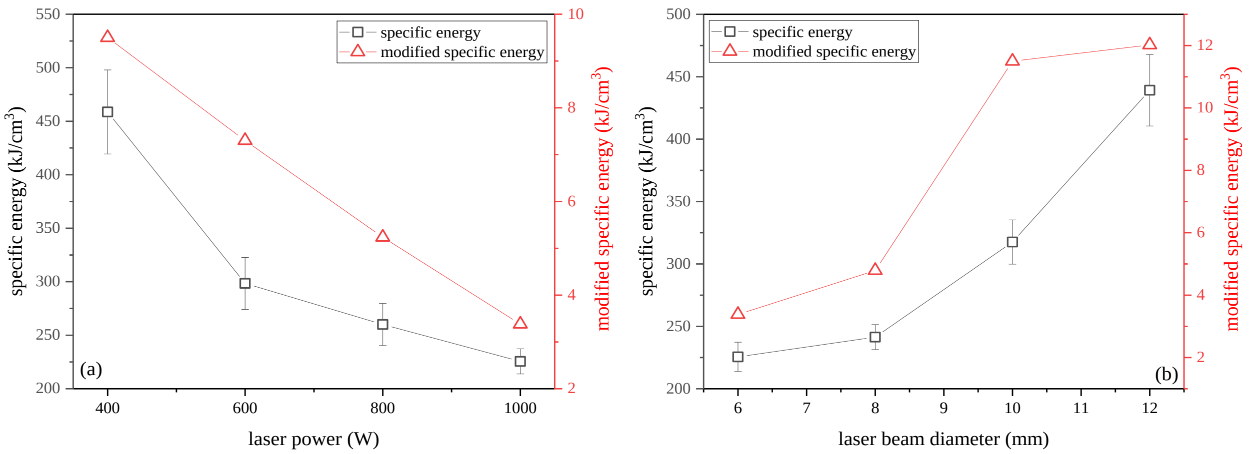

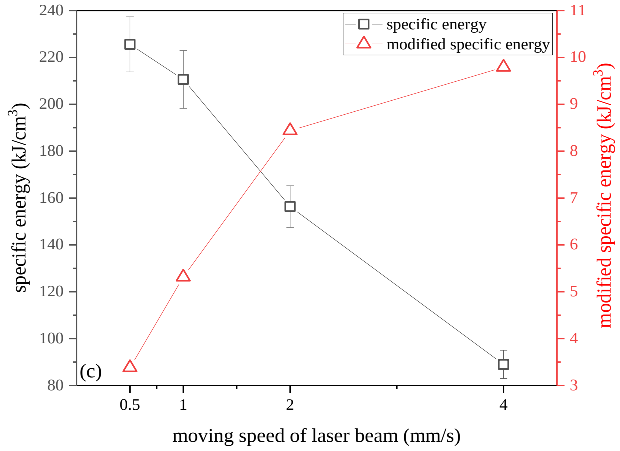

Fig. 10. SE and MSE versus (a) laser power (b) beam diameter (c) moving speed.

The MSE is based on the volume of cracked rock and the laser radiant energy applied on the rock surface. Fig. 10 (a) shows that the MSE nonlinearly decreases from 9.50 kJ/cm^3 to 3.38 kJ/cm^3 when the laser power is increased from 400 W to 1000 W, which indicates that less thermal energy is needed to crack the same amount of rock by using higher power laser. That is to say, the higher the laser irradiation power, the more efficient the thermal fracturing gets. Fig. 10 (b) illustrates the variation of MSE with laser beam diameter and the MSE is nonlinearly increased with an increasing laser beam diameter. For instance, the MSE increases from 3.38 kJ/cm^3 with a laser beam diameter of 6mm to about 12.02 kJ/cm^3 for a 12mm diameter of laser beam. It is believed that the distance between the rock sample and cutting head should be close to the focal length of laser beam to improve the efficiency of thermal fracturing with a small diameter. Fig. 10 (c) presents the variation of MSE with the moving speed of laser beam. It is shown that the MSE also increases from 3.38 kJ/cm^3 to 9.79 kJ/cm^3 with an increasing moving speed of laser beam from 0.5 mm/s to 4.0 mm/s. It should be noted that the total thermal energy emitted from laser beam is different for different moving speed of laser beam because the required time varies with moving speed. The higher the moving speed of laser beam, the smaller the thermal energy emitted from laser beam to the rock sample. The MSE decreases with the increasing moving speed of laser beam because the less thermal energy is emitted from laser beam to the same irradiating area within the same irradiation time, which indicates that much more thermal energy and irradiation time is needed to keep on fracturing the granite sample. In addition, the MSE is observed to be about one or two orders of magnitude smaller than the specific energy. And the gap between SE and MSE also increases with the increased laser power, decreased laser beam diameter and moving speed. It means that thermal fracturing is more efficient than well drilling when using laser beam.

To further discuss the influences of different irradiation parameters on MSE and SE, a concept of power density is introduced and it is defined as the ratio of laser power to the irradiation area on the target surface with the diameter that is equal to that of the laser beam irradiated on the rock surface. The laser power density varies only with the laser power and laser beam diameter as the irradiation time does not change in these experiments. However, laser power density also varies with moving speed of laser beam, the moving speed is not considered to transfer into power density in this paper since large divergence is observed between SE/MSE and power density induced from moving speed of laser beam. Fig. 11 shows the variations of MSE and SE with power density summaries from the experiments. Both MSE and SE are observed to decrease logarithmically with increased power density, which indicates that higher power density should be used in order to improve the efficiency of thermal fracturing and drilling. Also in the Fig. 11 (a) and (b), detailed curve fitting parameters of the experimental data are included in the tables in the corresponding figures.

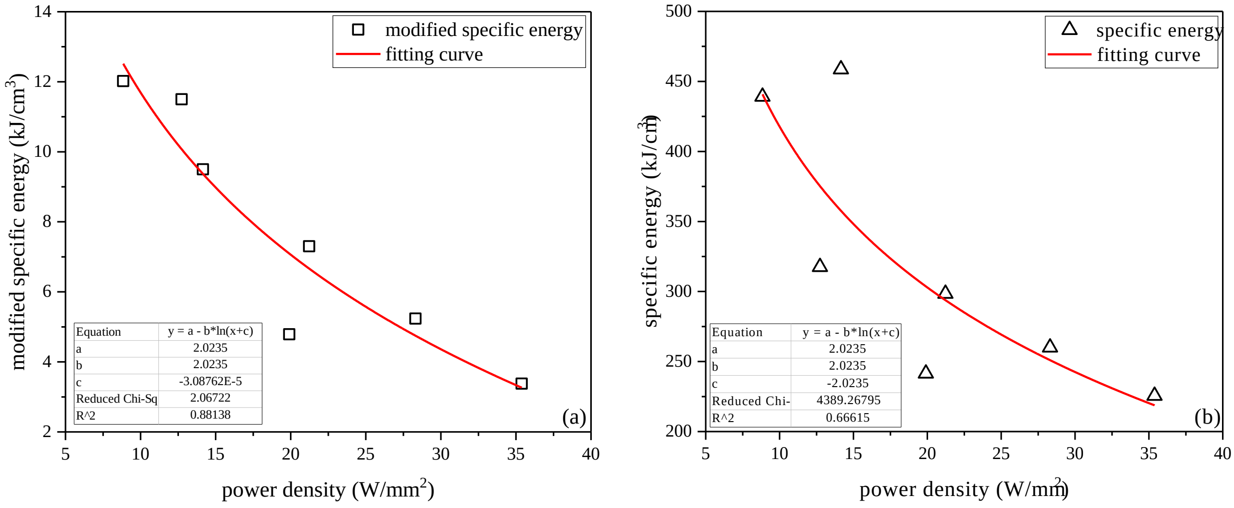

Fig. 11. MSE (a) and SE (b) versus power density.

3.3. Grooving kerf and open porosity

3.3.1. Grooving kerf

The real-time observation of the forming process of grooving kerf is not easy through the visible-light testing technology owing to the strong reflection caused by rock sample with super-high temperature. The grooving kerf caused by laser irradiation is investigated after the irradiated rock sample is cooled naturally to the room temperature. Fig. 12 shows the images of the specimens taken at the room temperature and clear grooving kerfs can be found at the center of each sample. Also detailed dimensions of kerf created by the laser beams under various laser irradiation conditions are illustrated. It is seen that both the depth and width of the grooving kerf increase with increasing laser power from Fig. 12 (a).The depth and width of grooving kerf increase from 4.90 mm and 6.29 mm at laser power level of 400 W to 10.69 mm and 8.40 mm respectively when the laser power is increased to 1000 W. The depth of kerf is increased by about 118.2% and the width is increased by about 33.5%. For the same laser beam diameter and the same moving speed, the laser cutting is much deeper when the laser power is increased. However, when the laser beam is increased with the same laser power and moving speed, a wider and shallow grooving kerf is cut by the laser beam as can be seen from Fig. 12 (b). The width of grooving kerf is increased from 8.40 mm to 12.67 mm and the depth is reduced from 10.69 mm to 6.22 mm when the laser beam diameter is increased from 6 mm to 12 mm. This is understandable as the laser beam diameter is increased, a wider area is heated up, but with the same laser power, the power density at the irradiation spot is reduced and results in a shallow grooving kerf remained after laser irradiation. Finally, when the moving speed is increased, one can see that both grooving kerf depth and width are reduced given the same laser beam and diameter, as shown in Fig. 12 (c). For instance, the depth and width of grooving kerf decrease from 10.69 mm and 8.40 mm to 3.91 mm and 5.56 mm respectively when the moving speed of laser beam is increased from 0.5 mm/s to 4.0 mm/s. The reason is that when the moving speed of laser beam is increased, less irradiation time is needed to cover the same length of the sample, therefore much less energy is injected into the sample and less damage to the specimen is incurred.

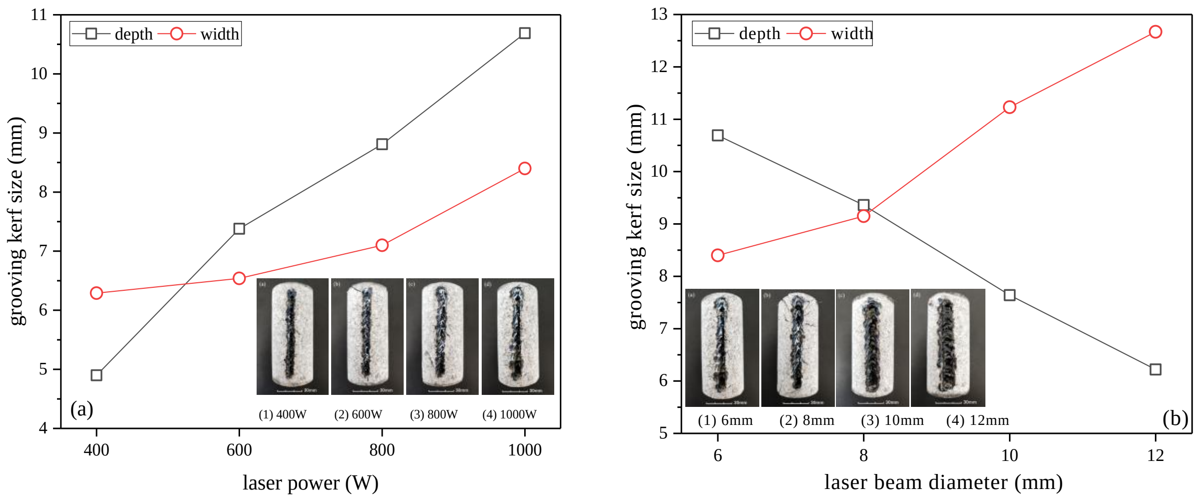

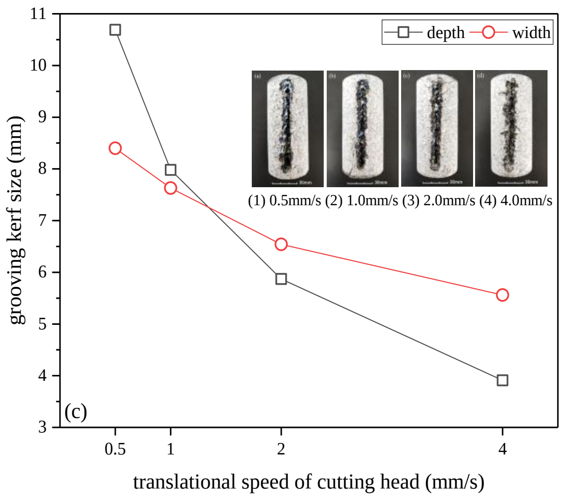

Fig. 12. Grooving kerf size versus (a) laser power (b) beam diameter (c) moving speed.

3.3.2. Open porosity

The porosity can generally be classified into total porosity, open porosity (OP) and connected porosity. The open porosity is defined as the fraction of the volume that is occupied by the fluid in the interconnected porous network to the total bulk volume of the porous solid [36]. It should be noted that the non-interconnected air voids trapped in the porous solid are not included in the OP, because it only considers the proportion of the voids that are communicated with the outside of the porous solid. The OP is an important parameter related to the effective properties of the fluid saturating the interconnected pores to the effective properties of the porous solids. Salissou et al [37] introduced a method to measure the OP of porous solids by using a simple apparatus of gas porosimeter and presented the theory behind this method to analyze the OP and its precision. This method was based on the measurement of four masses at different static pressures from which the OP is derived by using the ideal gas law. The most challenge part of this method is that the mass of gas under different pressure with the volume of porous solid must be readable. Owing to the high density of granite rock and very low porosity of the sample, it is impossible to employ this method for the OP measurement of the sample. Therefore, another method proposed by Chaki et al [38] is applied to measure the OP of thermally damaged granite rock, which can be derived from mass measurements of dry, water-saturated and immersed rock samples. It is found that the OP is significantly increased when the granite sample is heated to 500 ^{o}C and 600 ^{o}C.

All of the rock samples are saturated in a vacuum chamber with a mechanical pump in order to get saturation results accurately, as shown in Fig. 13. Firstly, the original rock samples are put into the drying oven at a temperature of 105 ^{o}C for 24 h to evaporate the water within the sample. The vacuum pump saturation apparatus is employed to saturate the original granite samples before irradiation. The mass of dry original rock samples is measured, and the saturated water contents of the rock samples are therefore obtained. Secondly, the irradiated granite samples are put into the drying oven with a preset temperature of 105 ^{o}C for 24 h to eliminate the water contained in the sample. The mass of the dry irradiated rock samples is then measured after the rock samples are cooled to room temperature. Finally, the dry irradiated rock samples are then saturated in the vacuum pump saturation apparatus for 12 h to drain away the air trapped in the rock samples. The mass of the saturated rock samples irradiated by fiber laser are tested through balance with high precision.

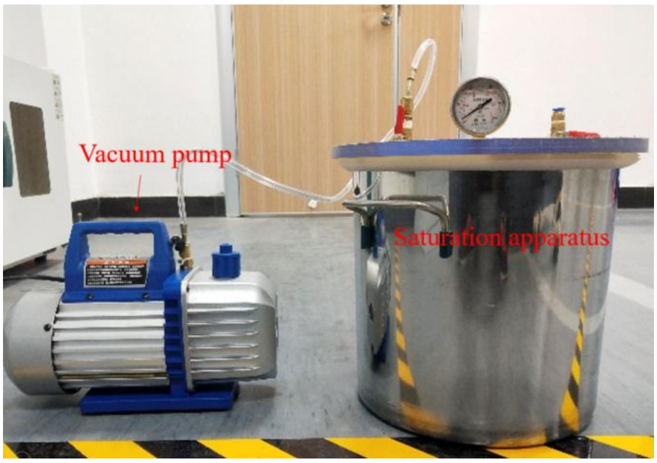

Fig. 13. Vacuum pump saturation apparatus.

The changes of mass of dry and saturated rock samples with laser power, laser beam diameter and moving speed of laser beam are illustrated in Table 7 - Table 9 respectively. In addition, the volumes of cracked rock are also calculated.

Table 7. Volume of cracked rock versus laser power.

Laser power (W)	Mass of dry rock ($\times 10^{-3}$ kg)	Mass of saturated rock ($\times 10^{-3}$ kg)	Volume of cracked rock cm^3
400	508.32	510.51	1.47
600	503.42	505.96	1.83
800	506.64	510.37	3.01
1000	503.55	508.24	3.97

Table 8. Volume of cracked rock versus laser beam diameter.

Laser beam diameter (mm)	Mass of dry rock ($\times 10^{-3}$ kg)	Mass of saturated rock ($\times 10^{-3}$ kg)	Volume of cracked rock cm^3
6	503.55	508.24	3.97
8	506.85	511.03	3.46
10	506.67	509.59	2.20
12	505.38	508.23	2.13

Table 9. Volume of cracked rock versus moving speed of laser beam.

Moving speed (mm/s)	Mass of dry rock ($\times 10^{-3}$ kg)	Mass of saturated rock ($\times 10^{-3}$ kg)	Volume of cracked rock cm^3
0.5	503.55	508.24	3.97
1	507.66	510.16	1.78
2	503.87	505.50	0.91
4	504.47	505.67	0.48

As shown in Table 7, volumes of cracked rock caused by laser irradiation are observed to increase with increasing laser power. From 400 W to 600 W, the volume of cracked rock increases gradually with a weak variation. This variation becomes considerably large between 600 W and 1000 W. For instance, the volume of cracked rock increases from 1.83 cm^3 with laser power of 600 W to 3.97 cm^3 with laser power of 1000 W, which stands for an increase of 116.9% comparing with that of 24.5% when the laser power increases from 400 W to 600 W. The volumes of cracked rock nonlinearly decrease when both laser beam diameter and moving speed of laser beam increase as listed in Table 8 and Table 9, which shows the laser beam diameter has a smaller impact on the volume of cracked rock than the moving speed of laser beam. For instance, the volume of cracks decreases from 3.97 cm^3 to 2.13 cm^3 when the laser beam diameter increases from 6mm to 12 mm. Meantime, the volume of cracked rock decreases from 3.97 cm^3 to 0.48 cm^3 when the moving speed of laser beam increases from 0.5 mm/s to 4.0 mm/s.

According to the definition of open porosity described by Eq. (4), the variations of OP of the irradiated rock sample against laser power, laser beam diameter and moving speed of laser beam are investigated and plotted in Fig. 14. The OP nonlinearly increases with increasing laser power. As shown in Fig. 14 (a), the OP gradually increases from 0.75% to 0.94% as the laser power increases from 400 W to 600 W. When the laser power is above 600 W, further increase in the laser power has an increased impact on OP. For instance, the increased percentage in OP changes from 0.94% to 2.03% when the laser power changes from 600 W to 1000 W, as shown in Table 7. As expected from Fig. 14 (b)-(c), both diameter and moving speed of laser beam have detrimental impact on the OP. However, the moving speed of laser beam has a greater effect on the OP than the laser beam diameter. For instance, the OP decreases from 2.03% to 1.09%, and from 2.03% to 0.25% when the laser beam diameter and moving speed increase from 6 mm to 12 mm and 0.5 mm/s to 4 mm/s respectively. The results are in good agreement with the impact that laser power, laser beam diameter and moving speed of laser beam have on the volumes of cracked rock.

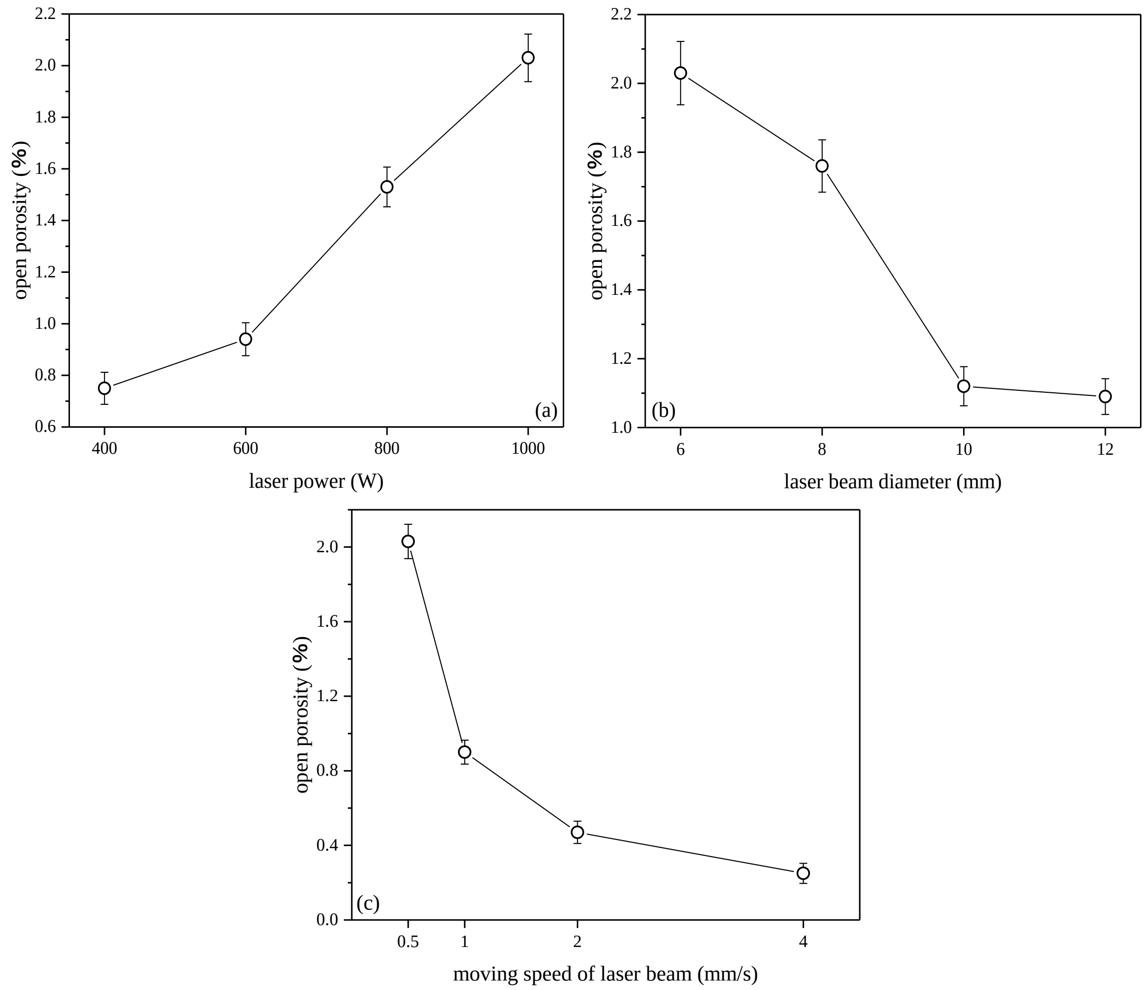

Fig. 14. Open porosity versus (a) laser power (b) beam diameter (c) moving speed.

4. Conclusions

This paper investigates the impact of different laser irradiation conditions including laser power, laser beam diameter and moving speed of laser beam on temperature, specific energy, modified specific energy and open porosity of the granite rock. The mass of removed and cracked rock, sizes of grooving kerfs are also studied and reported quantitatively. The key finding and conclusions are summarized as follows:

(1) Both the maximum rock temperature and the area with high rock temperature are increased by higher laser power, smaller laser beam diameter and longer irradiation time. However, the impact of the laser irradiation conditions on the area with high rock temperature is more significant than that

on rock temperature gradient.

(2) The mass of removed rock and the mass of cracked rock from the specimen due to laser irradiation are nonlinearly increased by increasing laser power, decreasing diameter and moving speed of laser beam. The variations in specific energy and modified specific energy caused by laser power, diameter and moving speed of laser beam are similar, but the values of modified specific energy are one or two orders of magnitude lower than the specific energy under the same laser irradiation conditions. Both of them are nonlinearly reduced with power density.

(3) Higher power laser irradiation cuts the granite rock sample deeper and wider and causes more damages to the sample. Both depth and width of the grooving kerf are increased with the laser power, but the depth of grooving kerf decreases when the laser beam diameter increases, which is opposite to that of the width. Both the width and depth of grooving kerf decrease when the moving speed of laser beam increases. The open porosity of irradiated rock increases with increasing laser power, decreasing beam diameter and moving speed of laser beam.

Acknowledgements

The authors wish to thank the National Natural Science Foundation of China (51978653) and Higher Education Discipline Innovation Project (B14021) for supporting this research.

References:

[1] Z.J. Feng, Y.S. Zhao, A.C. Zhou, N. Zhang, Development program of hot dry rock geothermal resource in the Yangbajing Basin of China, Renew Energ 39(1) (2012) 490-495.

[2] Z.J. Wan, Y.S. Zhao, J.R. Kang, Forecast and evaluation of hot dry rock geothermal resource in China, Renew Energ 30(12) (2005) 1831-1846.

[3] S.Y. Pan, M.Y. Gao, K.J. Shah, J.M. Zheng, S.L. Pei, P.C. Chiang, Establishment of enhanced geothermal energy utilization plans: Barriers and strategies, Renew Energ 132 (2019) 19-32.

[4] B.B. Zheng, J.P. Xu, T. Ni, M.H. Li, Geothermal energy utilization trends from a technological paradigm perspective, Renew Energ 77 (2015) 430-441.

[5] J.L. Zhu, K.Y. Hu, X.L. Lu, X.X. Huang, K.T. Liu, X.J. Wu, A review of geothermal energy resources, development, and applications in China: Current status and prospects, Energy 93 (2015) 466-483.

[6] Y. Feng, X. Chen, X.F. Xu, Current status and potentials of enhanced geothermal system in China: A review, Renew Sust Energ Rev 33 (2014) 214-223.

[7] L.B. Hu, A. Ghassemi, J. Pritchett, S. Garg, Characterization of laboratory-scale hydraulic fracturing for EGS, Geothermics 83 (2020).

[8] W.W. Ma, Y.D. Wang, X.T. Wu, G. Liu, Hot dry rock (HDR) hydraulic fracturing propagation and impact factors assessment via sensitivity indicator, Renew Energ 146 (2020) 2716-2723.

[9] Y.S. Zhao, Z.J. Feng, Y. Zhao, Z.J. Wan, Experimental investigation on thermal cracking, permeability under HTHP and application for geothermal mining of HDR, Energy 132 (2017) 305-314.

[10] Y.S. Zhao, Z.J. Feng, B.P. Xi, Z.J. Wan, D. Yang, W.G. Liang, Deformation and instability failure of borehole at high temperature and high pressure in Hot Dry Rock exploitation, Renew Energ 77 (2015) 159-165.

[11] X. Wei, Z.J. Feng, Y.S. Zhao, Numerical simulation of thermo-hydro-mechanical coupling effect in mining fault-mode hot dry rock geothermal energy, Renew Energ 139 (2019) 120-135.

[12] W.T. Yin, Y.S. Zhao, Z.J. Feng, Experimental research on the rupture characteristics of fractures subsequently filled by magma and hydrothermal fluid in hot dry rock, Renew Energ 139 (2019) 71-79.

[13] G.Y. Wang, D. Yang, Y.S. Zhao, Z.Q. Kang, J. Zhao, X.D. Huang, Experimental investigation

on anisotropic permeability and its relationship with anisotropic thermal cracking of oil shale under high temperature and triaxial stress, Appl Therm Eng 146 (2019) 718-725.

[14] Y.B. Huang, Y.J. Zhang, Z.W. Yu, Y.Q. Ma, C. Zhang, Experimental investigation of seepage and heat transfer in rough fractures for enhanced geothermal systems, Renew Energ 135 (2019) 846-855.

[15] Y.J. Zhang, Y.Q. Ma, Z.J. Hu, H.L. Lei, L. Bai, Z.H. Lei, Q. Zhang, An experimental investigation into the characteristics of hydraulic fracturing and fracture permeability after hydraulic fracturing in granite, Renew Energ 140 (2019) 615-624.

[16] P.S. Wei, T.C. Chao, Prediction of pore size in high power density beam welding, Int J Heat Mass Tran 79 (2014) 223-232.

[17] Y.M. Zhang, Z.H. Shen, X.W. Ni, Modeling and simulation on long pulse laser drilling processing, Int J Heat Mass Tran 73 (2014) 429-437.

[18] T. Sakurai, H. Chosrowjan, T. Somekawa, M. Fujita, H. Motoyama, O. Watanabe, Y. Izawa, Studies of melting ice using CO2 laser for ice drilling, Cold Reg Sci Technol 121 (2016) 11-15.

[19] Y.Q. Yang, Z. Chen, Y.W. Zhang, Melt flow and heat transfer in laser drilling, Int J Therm Sci 107 (2016) 141-152.

[20] Y.W. Ai, P. Jiang, X.Y. Shao, P.G. Li, C.M. Wang, A three-dimensional numerical simulation model for weld characteristics analysis in fiber laser keyhole welding, Int J Heat Mass Tran 108 (2017) 614-626.

[21] Y.W. Ai, P. Jiang, X.Y. Shao, P.G. Li, C.M. Wang, G.Y. Mi, S.N. Geng, Y. Liu, W. Liu, The prediction of the whole weld in fiber laser keyhole welding based on numerical simulation, Appl Therm Eng 113 (2017) 980-993.

[22] B.R. Jurewicz, Rock Excavation with Laser Assistance, Int J Rock Mech Min 13(7) (1976)

207-219.

[23] M. Ahmadi, M.R. Erfan, M.J. Torkamany, G.A. Safian, The effect of interaction time and saturation of rock on specific energy in ND:YAG laser perforating, Opt Laser Technol 43(1) (2011) 226-231.

[24] M.R. Erfan, K. Shahriar, M. Sharifzadeh, M. Ahmadi, M.J. Torkamany, Moving perforation of rocks using long pulse Nd:YAG laser, Opt Laser Eng 94 (2017) 12-16.

[25] M.X. Hu, Y. Bai, H.W. Chen, B.L. Lu, J.T. Bai, Engineering characteristics of laser perforation with a high power fiber laser in oil and gas wells, Infrared Phys Techn 92 (2018) 103-108.

[26] H. Kariminezhad, H. Amani, M. Moosapoor, A laboratory study about laser perforation of concrete for application in oil and gas wells, J Nat Gas Sci Eng 32 (2016) 566-573.

[27] R. Keshavarzi, Application of High Power Lasers in Perforation and Fracture Initiation of Oil and Gas Wells, Laser Eng 21(3-4) (2011) 149-167.

[28] M.Y. Li, B. Han, Q. Zhang, S.Y. Zhang, Q.K. He, Investigation on rock breaking for sandstone with high power density laser beam, Optik 180 (2019) 635-647.

[29] Z.H. Lyu, X.Z. Song, G.S. Li, Y. Shi, R. Zheng, G.S. Wang, Y. Liu, Investigations on thermal spallation drilling performance using the specific energy method, J Nat Gas Sci Eng 54 (2018) 216-223.

[30] R.M. Miranda, Structural analysis of the heat affected zone of marble and limestone tiles cut by CO2 laser, Mater Charact 53(5) (2004) 411-417.

[31] G.K.L. Ng, P.L. Crouse, L. Li, An analytical model for laser drilling incorporating effects of exothermic reaction, pulse width and hole geometry, Int J Heat Mass Tran 49(7-8) (2006) 1358-1374.

[32] J. Shin, J. Mazumder, Numerical and experimental study on the effect of the pulse format in

laser drilling, J Laser Appl 28(1) (2016).

[33] F. Yan, Y.F. Gu, Y.J. Wang, C.M. Wang, X.Y. Hu, H.X. Peng, Z.L. Yao, Z. Wang, Y. Shen, Study on the interaction mechanism between laser and rock during perforation, Opt Laser Technol 54 (2013) 303-308.

[34] Y. Wang, Y. Shi, J. Jiang, G. Zhou, Z. Wang, Experimental study on modified specific energy, temperature field and mechanical properties of Xuzhou limestone irradiated by fiber laser, Heat and Mass Transfer 56(1) (2020) 161-173.

[35] T.J. Sullivan, Introduction to Uncertainty Quantification, Springer, Switzerland, 2015.

[36] J.F. Allard, N. Atalla, Propagation of Sound Porous Media: Modelling Sound Absorbing Material, John Wiley & Sons Ltd, Singapore, 2009.

[37] Y. Salissou, R. Panneton, Pressure/mass method to measure open porosity of porous solids, J Appl Phys 101(12) (2007).

[38] S. Chaki, M. Takarli, W.P. Agbodjan, Influence of thermal damage on physical properties of a granite rock: Porosity, permeability and ultrasonic wave evolutions, Constr Build Mater 22(7) (2008) 1456-1461.

Credit Author Statement

The authors confirm contributions to the paper as follows: research concept and design: Yijiang Wang, Guoqing Zhou; experimental data collection: Jinyi Jiang; analysis and interpretation: Zeyuan Xu, Xiaofeng Zheng, Yijiang Wang, Jo Darkwa. All authors reviewed the results and approved the final version of the manuscript.

Declaration of Interest Statement

The authors declare that they have no known competing financial interests or personal relationships that could have appeared to influence the work reported in this paper.